# Central-Upwind Schemes for the Boussinesq Paradigm Equations

Alina Chertock, Christo Christov and Alexander Kurganov

**Abstract** We develop a new accurate and robust numerical method for the Boussinesq paradigm equation (BPE). To design the method we first introduce a change of variables, for which the BPE takes the form of a nonlinear wave equation with the global pressure, and rewrite the wave equation as a system of conservation laws with a global flux. We then apply a Godunov-type central-upwind scheme together with an efficient FFT-based elliptic solver to the resulting system. Making use of the new scheme, we investigate the propagation of one- and two-dimensional solitary waves of BPE and identify their solitonic behavior.

## 1 Introduction

One of the most important events in mathematical physics was the discovery in the 1960s [16] that the nonlinear waves can behave as particles. The localized waves which can retain their identity during interaction appear to be a very adequate model for particles, especially if some mechanical quantities (such as mass, momentum, energy) are conserved by the governing system of equations. In the case when the system has an infinite number of conservation laws, the "permanent" localized waves are called *solitons*. In the past five decades, a multitude of deep mathematical results were obtained for solitons, and a plethora of analytical solutions found for

Alina Chertock
Department of Mathematics, North Carolina State University, Raleigh, NC 27695, USA, e-mail: chertock@math.ncsu.edu

Christo Christov
Department of Mathematics, University of Louisiana, Lafayette, LA 70504, USA, e-mail: christov@louisiana.edu

Alexander Kurganov
Mathematics Department, Tulane University, New Orleans, LA 70118, USA, e-mail: kurganov@math.tulane.edu

systems of interacting solitons. As it should have been expected, most of the physical systems are not fully integrable, and for them (even in one space dimension) only numerical approaches can lead to unearthing the pertinent physical mechanisms of the interactions (see, e.g., [4, 6] and references therein).

The overwhelming majority of the analytical and numerical results obtained so far are for the one-dimensional (1-D) case, while in the multiple number of space dimensions, much less can be achieved analytically, and almost nothing is known about the unsteady solutions that involve interactions, especially when full-fledged Boussinesq equations are involved. In the case when one of the fourth-order spatial derivatives can be neglected (the Kadomtsev-Petviashvili equation), two-dimensional (2-D) waves have been found. Being periodic in one of the spatial dimensions, the latter are not truly 2-D waves, localized in both direction. Thus the problem for the Boussinesq equation with fourth-order derivatives in both spatial directions, still awaits it solution.

The difficulties in the multidimensional cases are connected with the unboundedness of the region, and with the slow decay of the solution at infinity. For this reason, the first case to undergo investigation is when the wave profile is stationary in a frame moving with a prescribed phase speed. The shape of the stationary moving wave was reliably computed in [2] using a specialized Galerkin spectral technique, which showed that the decay at infinity is algebraic rather than exponential. A perturbation technique recently developed in [5] confirmed the findings of [2] and put the stationary problem on more rigorous analytical ground.

Upgrading the numerical approach to the unsteady 2-D case is non-trivial, and several different techniques are to be developed, in order to obtain reliable description of the mechanics and physics of the processes involved. The essential properties of the numerical method in this case is to be very efficient computationally, because of the sheer size of the problem: the computational box must be large enough to allow for a good approximation of the localized solution, and the grid must be fine enough to reduce the truncation error. The conservative schemes used in [4, 6] (and in the works of other authors) are not easily extended to 2-D cases, and require an excessive amount of computational time.

The purpose of the present paper is to apply the "machinery" of modern finite volume methods, Godunov-type central-upwind schemes [8, 9, 11, 13], to the BPE and to numerically study their solitary wave solutions.

We first outline the scheme for the 1-D BPE and then proceed to trace the evolution of a 2-D profile described in [5]. This is the first and utmost verification of the "solitonic" properties of the 2-D shapes, before they can be used in computations aimed at the investigation of their collision properties.

## 2 Boussinesq Paradigm Equation

When Boussinesq derived his famous equation [1], he demonstrated that the nonlinearity can balance dispersion and lead to the existence of waves of permanent shape

that propagate in quite similar fashion as the profiles of the d'Alembert solution of the wave equation. Unfortunately, Boussinesq did some additional (and as it turns out) unnecessary assumptions, which rendered his equation incorrect in the sense of Hadamard. An overview of the different Boussinesq equations can be found in [6] (see also references therein). The accurate derivation of the Boussinesq system can be found, e.g., in [4]. In nutshell, Boussinesq's's Boussinesq Equation (BBE) lacks the mixed fourth derivative, which was the cause of it incorrectness. In order to distinguish the equation to which a consistent application of Boussinesq idea would have led, the latter is called Boussinesq Paradigm Equation (BPE). The essential mathematical difference between BBE and BPE is that the former is fully integrable (although incorrect) and the latter is not (although, it is the physically pertinent and mathematically correct model). The BPE furnishes one of those examples, which necessitates an efficient numerical treatment as a precondition for a deeper physical understanding of the problem.

The BPE is a 2-D amplitude equation:

$$w_{tt} = \Delta \left[ w - \alpha w^2 + \beta_1 w_{tt} - \beta_2 \Delta w \right], \tag{1}$$

where $w$ is the surface elevation, $\beta_1, \beta_2 > 0$ are two dispersion coefficients, and $\alpha$ is an amplitude parameter. As it has been already mentioned, the main difference between equation (1) and the BBE is that now $\beta_1 \neq 0$.

It has been recently shown in [2, 5] that the 2-D BPE admits stationary soliton solutions as well. Even though no analytical formula for these solutions is available, they can be accurately constructed using either a perturbation or a Galerkin spectral method. However, the stability of the 2-D solitons has still been an open problem, and will be addressed in the present work.

The situation is much more amenable with the 1-D BPE:

$$w_{tt} = \left[ w - \alpha w^2 + \beta_1 w_{tt} - \beta_2 w_{xx} \right]_{xx}, \tag{2}$$

for which it has been shown (see [4] for references) that it admits a one-parameter family of soliton solutions given by

$$w^{\text{s}}(x,t;c) = -\frac{3}{2} \frac{c^2 - 1}{\alpha} \text{sech}^2 \left( \frac{x - ct}{2} \sqrt{\frac{c^2 - 1}{\beta_1 c^2 - \beta_2}} \right), \tag{3}$$

where $c$ is the phase speed of the stationary propagating 1-D localized wave. Although, equation (2) is not fully integrable, the extensive numerical investigation from [6] based on a conservative difference scheme, succeeded to show that in its main aspects, it behaves as its fully integrable "cousin", the BBE. Note that a solution of the above type exists for $|c| > \max\{1, \sqrt{\beta_2/\beta_1}\}$ or $|c| < \min\{1, \sqrt{\beta_2/\beta_1}\}$. The first case comprises of the so-called "supercritical" solitons, while the latter encompasses the "subcritical" ones. In the latter case, the physically relevant phase speeds are those that are significantly smaller than the threshold $\min\{1, \sqrt{\beta_2/\beta_1}\}$, because close to it, the soliton support becomes very short, and the main Boussinesq assumption about waves being long is violated. Moreover, it was shown in [3, 4] that

the subcritical solitons are less stable and tend not to preserve their shape upon collisions. For this reason, in the present parer, which is devoted to the development of a new numerical approach, we consider the supercritical shapes in 1-D, which exhibit remarkable stability as their identity is preserved through nonlinear interactions.

The goal of this paper is to develop an efficient and accurate numerical method for the 1-D and 2-D BPEs as well as to numerically study the stability and other properties of their soliton solutions. Our numerical method is designed in several steps. First, we introduce a new variable $\rho := w - \beta_1 w_{xx}$ (in 1-D) or $\rho := w - \beta_1 \Delta w$ (in 2-D), for which the BPE takes the form of a nonlinear wave equation. We then introduce another new variable, the "momentum" $m$ (in 1-D), or two new variables, the $x$- and $y$-"momenta" $m$ and $n$ (in 2-D), and rewrite the obtained wave equation as a system of conservation laws with global fluxes. The resulting system is numerically solved by a second-order central-upwind scheme, proposed in [11] and further improved in [9, 13] and [8], together with an efficient FFT-based elliptic solver used to recover $w$ from available values of $\rho$. The selection of the central-upwind scheme is motivated by its superb properties of this Riemann-problem-solver-free method—efficiency, accuracy and robustness, demonstrated in a wide variety of applications (see, e.g., [8] and references therein), including the models with global fluxes: the incompressible Navier-Stokes equations, [9, 12], and the traffic flow model with Arrhenius look-ahead dynamics, [10].

The rest of the paper is organized as follows. In Sect. 3, we describe the 1-D central-upwind scheme and numerically study stability of the 1-D solitons for different values of $c$ (in (3)) as well as their interactions and emergence out of general initial data. In Sect. 4, we use the 2-D extension of the central-upwind scheme to simulate the time evolution of 2-D solitons and to numerically study their stability.

## 3 Scheme and Algorithm for the 1-D BPE

We start by making a change of variables and defining a new variable $\rho$ as

$$\rho = w - \beta_1 w_{xx}. \tag{4}$$

In terms of this new variable, the BPE (2) takes the form of a nonlinear wave equation:

$$\rho_{tt} = p(\rho, w)_{xx}, \quad p(\rho, w) := \frac{\beta_2}{\beta_1}\rho + \left(1 - \frac{\beta_2}{\beta_1}\right)w - \alpha w^2, \tag{5}$$

in which the dependence of the "pressure" $p$ on the "density" $\rho$ is global. Next, we introduce another new variable, the "momentum" $m$, and rewrite the nonlinear wave equation (5) as a system of conservation laws for the variable $\mathbf{U} := (\rho, m)^T$ with a global flux function $\mathbf{F}(\mathbf{U}) = (m, p(\rho, w(\rho)))^T$:

$$\begin{cases} \rho_t + m_x = 0, \\ m_t + p(\rho, w)_x = 0, \end{cases} \tag{6}$$

where $p$ is defined in (5) and the dependence of $w$ on $\rho$ is given by the modified Helmholtz equation (4).

We then design a numerical method for the system (6), (4) using the following approach: the system (6) is solved by the second-order central-upwind scheme from [8], while the modified Helmholtz equation (4) is solved using the FFT-based elliptic solver. The details on our numerical method are provided in Sect. 3.1.

### 3.1 Description of the 1-D Numerical Method

We assume that the system (6) is augmented with (smooth) initial conditions and periodic boundary conditions (in 1-D, an extension of the proposed numerical method to the nonperiodic case is quite straightforward).

We introduce a spatial grid $\{C_j\}$, where $C_j := (x_{j-\frac{1}{2}}, x_{j+\frac{1}{2}})$ are the cells of a uniform size $\Delta x$ and denote the cell averages of $\mathbf{U}$ at time $t$ by

$$\overline{\mathbf{U}}_j(t) := \frac{1}{\Delta x} \int_{C_j} \mathbf{U}(x,t)\, dx.$$

According to the semi-discrete central-upwind scheme from [8], the cell averages are evolved in time by solving the following system of ODEs:

$$\frac{d}{dt}\overline{\mathbf{U}}_j(t) = -\frac{\mathbf{H}_{j+\frac{1}{2}}(t) - \mathbf{H}_{j-\frac{1}{2}}(t)}{\Delta x}, \tag{7}$$

where $\mathbf{H}_{j+\frac{1}{2}}$ is a numerical flux given by

$$\mathbf{H}_{j+\frac{1}{2}} = \frac{a_{j+\frac{1}{2}}^+ \mathbf{F}(\mathbf{U}_{j+\frac{1}{2}}^-) - a_{j+\frac{1}{2}}^- \mathbf{F}(\mathbf{U}_{j+\frac{1}{2}}^+)}{a_{j+\frac{1}{2}}^+ - a_{j+\frac{1}{2}}^-} + a_{j+\frac{1}{2}}^+ a_{j+\frac{1}{2}}^- \left[ \frac{\mathbf{U}_{j+\frac{1}{2}}^+ - \mathbf{U}_{j+\frac{1}{2}}^-}{a_{j+\frac{1}{2}}^+ - a_{j+\frac{1}{2}}^-} - \mathbf{q}_{j+\frac{1}{2}} \right]. \tag{8}$$

Here, the built-in "anti-diffusion" term (which corresponds to the reduced, compared with the original semi-discrete central-upwind scheme from [9], numerical dissipation) is

$$\mathbf{q}_{j+\frac{1}{2}} = \text{minmod}\left( \frac{\mathbf{U}_{j+\frac{1}{2}}^+ - \mathbf{U}_{j+\frac{1}{2}}^*}{a_{j+\frac{1}{2}}^+ - a_{j+\frac{1}{2}}^-}, \frac{\mathbf{U}_{j+\frac{1}{2}}^* - \mathbf{U}_{j+\frac{1}{2}}^-}{a_{j+\frac{1}{2}}^+ - a_{j+\frac{1}{2}}^-} \right), \tag{9}$$

where

$$\mathbf{U}_{j+\frac{1}{2}}^* = \frac{a_{j+\frac{1}{2}}^+ \mathbf{U}_{j+\frac{1}{2}}^+ - a_{j+\frac{1}{2}}^- \mathbf{U}_{j+\frac{1}{2}}^- - \left\{ \mathbf{F}(\mathbf{U}_{j+\frac{1}{2}}^+) - \mathbf{F}(\mathbf{U}_{j+\frac{1}{2}}^-) \right\}}{a_{j+\frac{1}{2}}^+ - a_{j+\frac{1}{2}}^-}, \tag{10}$$

and the minmod function,

$$\text{minmod}(z_1, z_2, \ldots, z_m) := \begin{cases} \min(z_1, z_2, \ldots, z_m), & \text{if } z_i > 0 \ \forall i = 1, \ldots, m, \\ \max(z_1, z_2, \ldots, z_m), & \text{if } z_i < 0 \ \forall i = 1, \ldots, m, \\ 0, & \text{otherwise,} \end{cases} \quad (11)$$

is applied in a componentwise manner.

In the numerical flux (8)–(10), $\mathbf{U}_{j+\frac{1}{2}}^{\pm} := \widetilde{\mathbf{U}}(x_{j+\frac{1}{2}})$ are used to denote the point values of a non-oscillatory interpolant $\widetilde{\mathbf{U}}$,

$$\widetilde{\mathbf{U}}(x,t) = \overline{\mathbf{U}}_j + (\mathbf{U}_x)_j(x - x_j), \qquad x_{j-\frac{1}{2}} < x < x_{j+\frac{1}{2}}, \quad \forall j, \qquad (12)$$

which is reconstructed at each time step from the previously computed cell averages $\{\overline{\mathbf{U}}_j(t)\}$. The second-order accuracy of the interpolant (12) is guaranteed provided $(\mathbf{U}_x)_j$ is (at least) first-order approximation of the derivative $\mathbf{U}_x(x_j, t)$. In all our numerical experiments, we have computed $(\mathbf{U}_x)_j$ using the minmod limiter (see, e.g., [14, 15]):

$$(\mathbf{U}_x)_j = \text{minmod}\left(2\frac{\overline{\mathbf{U}}_j - \overline{\mathbf{U}}_{j-1}}{\Delta x}, \frac{\overline{\mathbf{U}}_{j+1} - \overline{\mathbf{U}}_{j-1}}{2\Delta x}, 2\frac{\overline{\mathbf{U}}_{j+1} - \overline{\mathbf{U}}_j}{\Delta x}\right), \qquad (13)$$

where the minmod function is defined in (11).

Finally, $a_{j+\frac{1}{2}}^{\pm}$ are the local speeds of propagation, which can be estimated using the largest and the smallest eigenvalues of the Jacobian, see [8, 9]. Since the flux in the system (6) is global, we calculate the local speeds as follows:

$$a_{j+\frac{1}{2}}^{\pm} = \pm\max\left(\sqrt{p'(\rho_{j+\frac{1}{2}}^+)}, \sqrt{p'(\rho_{j+\frac{1}{2}}^-)}\right), \qquad (14)$$

where

$$p'(\rho) = \frac{\beta_2}{\beta_1} + \left(1 - \frac{\beta_2}{\beta_1}\right)w'(\rho) + 2\alpha w(\rho)w'(\rho),$$

and the derivative $w'(\rho)$ is calculated using the chain rule and equation (4):

$$w'(\rho) = \frac{w_x}{\rho_x} = \frac{w_x}{w_x - \beta_1 w_{xxx}}.$$

It should be observed that the values of $w$ and its derivatives at each time step are obtained from the given values of $\rho$ by solving the modified Helmholtz equation (4). Thanks to the periodic boundary conditions, equation (4) can be efficiently and highly accurately solved using a standard FFT-based elliptic solver.

*Remark 1.* Since the local speeds in (14) are symmetric, namely,

$$a_{j+\frac{1}{2}}^+ = -a_{j+\frac{1}{2}}^- =: a_{j+\frac{1}{2}}, \quad \forall j,$$

the flux formulae (8)–(10) are simplified to:

$$\mathbf{H}_{j+\frac{1}{2}} = \frac{1}{2}\left\{\mathbf{F}(\mathbf{U}^-_{j+\frac{1}{2}}) + \mathbf{F}(\mathbf{U}^+_{j+\frac{1}{2}})\right\} - \frac{a_{j+\frac{1}{2}}}{2}\left[\mathbf{U}^+_{j+\frac{1}{2}} - \mathbf{U}^-_{j+\frac{1}{2}} - \mathbf{q}_{j+\frac{1}{2}}\right], \quad (15)$$

$$\mathbf{q}_{j+\frac{1}{2}} = \mathrm{minmod}\left(\mathbf{U}^+_{j+\frac{1}{2}} - \mathbf{U}^*_{j+\frac{1}{2}}, \mathbf{U}^*_{j+\frac{1}{2}} - \mathbf{U}^-_{j+\frac{1}{2}}\right), \quad (16)$$

$$\mathbf{U}^*_{j+\frac{1}{2}} = \frac{1}{2}\left(\mathbf{U}^+_{j+\frac{1}{2}} + \mathbf{U}^-_{j+\frac{1}{2}}\right) - \frac{1}{2a_{j+\frac{1}{2}}}\left\{\mathbf{F}(\mathbf{U}^+_{j+\frac{1}{2}}) - \mathbf{F}(\mathbf{U}^-_{j+\frac{1}{2}})\right\}. \quad (17)$$

*Remark 2.* The ODE system (7) has to be solved by a stable and sufficiently accurate ODE solver. In our numerical experiments, we have used the third-order strong stability preserving (SSP) Runge-Kutta method from [7].

### 3.2 1-D Numerical Experiments

We apply the central-upwind scheme (7), (15)–(17) to the system (6). Our goal is to demonstrate stability of the soliton solutions (3) and to numerically verify whether they are attractors for general initial data. In all the 1-D numerical experiments below, we used the same set of parameters $\alpha, \beta_1$ and $\beta_2$, namely,

$$\alpha = -3, \ \beta_1 = 1.5, \ \beta_2 = 0.5.$$

This particular set was shown to correspond to the flow in a shallow layer [4], but in a paradigmatic sense, any other set of values for the dispersion can be used. If the ratio is kept $\beta_1/\beta_2 = 3$, the relevance to the shallow-layer case can still be shown, but for some stretched spatial coordinates.

**Example 1—Single Solitons**

We first consider the following initial datum:

$$w(x, 0) = w^{\mathrm{s}}(x, 0; 1.2), \quad (18)$$

which represents a single soliton at the initial time moment, which is then allowed to evolve according to the BPE. In this case, the soliton is expected to travel to the right with the constant speed of $c = 1.2$. We apply the proposed central-upwind scheme to the initial value problem (IVP) (2), (18). The snapshots of the solution, computed at different times on the uniform grid with $\Delta x = 100/512$, are plotted in Fig. 1(a). As one can see, the soliton is numerically stable as predicted in [3, 4].

Next, we take a different initial datum:

$$w(x, 0) = w^{\mathrm{s}}(x, 0; 5), \quad (19)$$

for which the soliton is still expected to travel to the right but with a much higher speed (since $c = 5$). Capturing the evolution of such fast soliton is quite a chal-
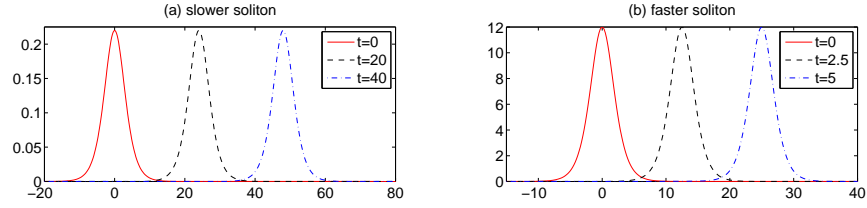
**Fig. 1** Numerical evolution of isolated solitons as solutions of (2)

lenging task since the energy functional is not positive definite. For example, the numerical scheme, presented in [6], failed on similar sets of initial data with $c > 2.1$ developing a nonlinear blowup when collision of solitons was considered. The solution, computed by the proposed central-upwind scheme at different times on the uniform grid with $\Delta x = 100/512$, is presented in Fig. 1(b). As one can observe, the scheme captures the evolution of the solitary waves correctly, no instabilities have developed and the quality of the solution is as good as in the previous case.

### Example 2—Interaction of Two Solitons

In this example, we simulate a nonlinear interaction of two solitons with different initial speeds. The initial profile is taken as the following superposition of two solitons:

$$w(x,0) = w^s(x+40,0;1.2) + w^s(x-50,0;-1.5), \qquad (20)$$

on the interval $[-150,120]$. The initial condition (20) and the solution at times $t = 15, 30, 40, 60$ and $100$, computed by the central-upwind scheme with $\Delta x = 270/2048$, are plotted in Fig. 2. As one can see, the higher soliton (initially located on the right) that travels with a negative phase velocity ($c = -1.5$) passes through the lower soliton which travels to the right ($c = 1.2$) after going through a nonlinear interaction. Evidently, the proposed method is capable of capturing the nonlinear soliton interaction with a high resolution. Juxtaposing the profiles before and after the interaction shows that they indeed have the solitonic property of shape preservation. The height, the support and the energy of each soliton are preserved with a high accuracy.
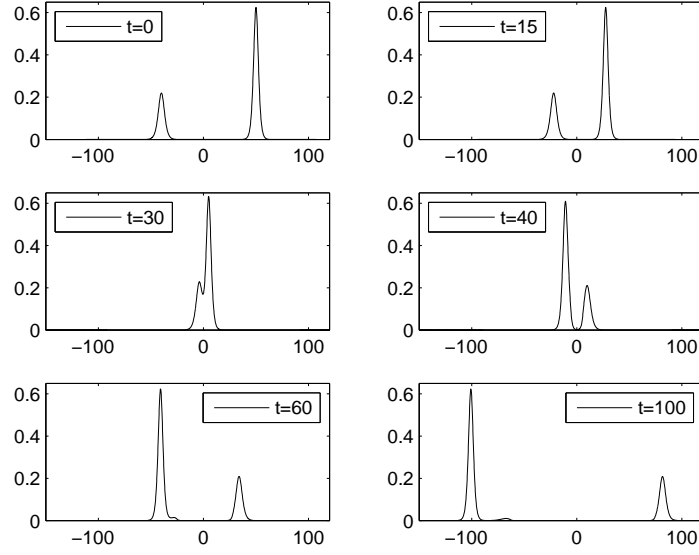
### Example 3—Arbitrary Initial Data

Finally, we consider equation (2) subject to arbitrary initial conditions:

$$w(x,0) = \text{sech}^2(0.5x), \quad w_t(x,0) \equiv 0. \qquad (21)$$

We call this solution "arbitrary" despite of its "sech" shape, because the phase speed is equal to zero, and the soliton $w^s(x,t;0)$ that corresponds to $c = 0$ has nothing to

**Fig. 2** Evolution of the numerical solution of (2), (20): interaction of two solitons

do with the particularly chosen "sech" shape (21). In this case, according to the analytical results for fully integrable systems, we expect two (or more) soliton solitons of type (3) to emerge out of this initial data. In Fig. 3, we plot the solution at times $t = 0, 2, 5, 10, 20$ and $30$, computed by the central-upwind scheme on a uniform grid with $\Delta x = 120/1024$. What can be clearly seen are two solitons branching from the initial data, each of them having a canonical soliton shape and moving with the phase speed that corresponds to its particular shape.

*Remark 3.* In all of the above 1-D numerical experiments, we have performed a mesh refinement convergence study and observed that the numerical solutions have been convergent.

## 4 2-D Numerical Experiments with the BPE

### 4.1 Setting for the 2-D Numerical Method

In this section, we consider the 2-D BPE (1). As in the 1-D case, we first make a change of variables and denote by $\rho$ the following function:

$$\rho = w - \beta_1 \Delta w. \tag{22}$$
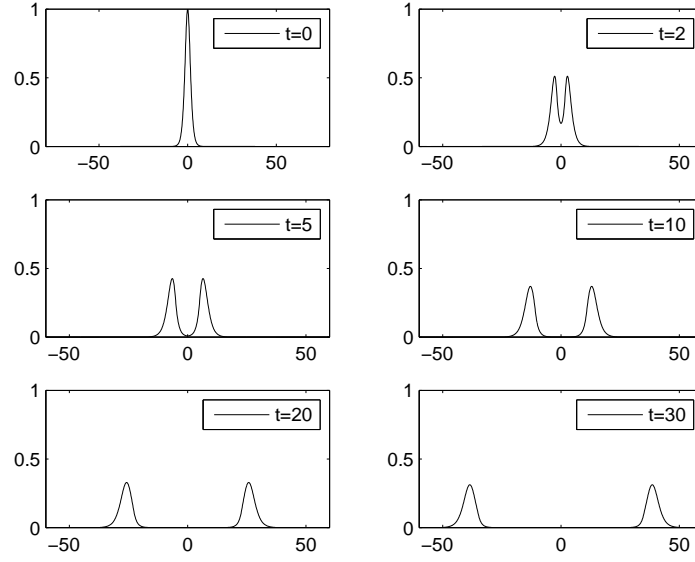
**Fig. 3** Two solitons emerging out of the initial data (21)

This allows one to rewrite the BPE (1) in the form of a nonlinear wave equation:

$$\rho_{tt} = \Delta p(\rho, w), \quad p(\rho, w) := \frac{\beta_2}{\beta_1}\rho + \left(1 - \frac{\beta_2}{\beta_1}\right)w - \alpha w^2. \tag{23}$$

Introducing two new variables, the $x$- and $y$-"momenta" $m$ and $n$, and rewriting the last equation as a system of conservation laws for $\mathbf{U} := (\rho, m, n)^T$ yields:

$$\begin{cases} \rho_t + m_x + n_y = 0, \\ m_t + p(\rho, w)_x = 0, \\ n_t + p(\rho, w)_y = 0. \end{cases} \tag{24}$$

The system (24) can be written in the following vector form:

$$\mathbf{U}_t + \mathbf{F}(\mathbf{U})_x + \mathbf{G}(\mathbf{U})_y = 0, \tag{25}$$

where the global flux functions $\mathbf{F}$ and $\mathbf{G}$ are given by $\mathbf{F}(\mathbf{U}) = (m, p(\rho, w(\rho)), 0)^T$ and $\mathbf{G}(\mathbf{U}) = (n, 0, p(\rho, w(\rho)))^T$, respectively, and the relation between the variables $\rho$ and $w$ is governed by the modified Helmholtz equation (22).

The numerical method for the resulting system is designed based on the same (as in the 1-D case) idea: the system (24) is numerically integrated by the 2-D version of the proposed central-upwind scheme, which can be found in, e.g., [8], while the modified Helmholtz equation (22) is solved using an FFT-based elliptic solver.

## 4.2 2-D Numerical Experiments

For definiteness, in the numerical experiments reported in this section, we consider equation (1) with $\alpha = 1, \beta_1 = 3, \beta_2 = 1$ subject to the initial data

$$w(x,y,0) = w^s(x,y - \eta,t;c) \tag{26}$$

which correspond to a soliton moving along the $y$-axis with velocity $c$. Because of the rotational symmetry of the operators in the BPE, any other case can be reduced to a case with only one nontrivial component of the phase speed. In [5], a comprehensive semi-analytical/semi-numerical solution was summarized as best-fit functions of the governing parameters. For $\beta_2 = 1$, the following best fit approximation given in [5] was presented for the shape of the 2-D soliton:

$$w^s(x,y,t;c) = f(x,y) + c^2[(1-\beta_1)g_a(x,y) + \beta_1 g_b(x,y)]$$
$$+ c^2[(1-\beta_1)h_1(x,y) + \beta_1 h_2(x,y)\cos(2\theta)],$$

where

$$f(x,y) = \frac{2.4(1+0.24r^2)}{\cosh(r)(1+0.095r^2)^{1.5}},$$

$$g_a(x,y) = -\frac{1.2(1-0.177r^{2.4})}{\cosh(r)|1+0.11r^{2.1}|}, \quad g_b(x,y) = -\frac{1.2(1+0.22r^2)}{\cosh(r)|1+0.11r^{2.4}|},$$

$$h_i(x,y) = \frac{a_i r^2 + b_i r^3 + c_i r^4 + v_i r^6}{1 + d_i r + e_i r^2 + f_i r^3 + g_i r^4 + h_i r^5 + q_i r^6 + w_i r^8}.$$

Here, $r = \sqrt{x^2+y^2}$, $\theta = \arctan(y/x)$, and the coefficients are: $a_1 = 1.03993$, $a_2 = 31.2172$, $b_1 = 6.80344$, $b_2 = -10.0834$, $c_1 = -0.22992$, $c_2 = 3.97869$, $d_1 = 12.6069$, $d_2 = 77.9734$, $e_1 = 13.5074$, $e_2 = -76.9199$, $f_1 = 2.46495$, $f_2 = 55.4646$, $g_1 = 2.45953$, $g_2 = -12.9335$, $h_1 = 1.03734$, $h_2 = 1.0351$, $q_1 = -0.0246084$, $q_2 = 0.628801$, $v_1 = 0.0201666$, $v_2 = -0.0290619$, $w_1 = 0.00408432$, $w_2 = -0.00573272$.

We first test our scheme on the case $c = 0$, when the solution has an exponential decay at infinity and hence is tightly localized. In this case, we take a computational domain $[-15,15] \times [-15,15]$, which is sufficiently large and hence the localized solution does not interact with the computational boundaries. The profile in this case is a standing soliton, and apart from the sheer validation significance, the computations are also purported to answer an important question: can the nonlinearity without motion keep this soliton from being annihilated by the diffusion?

We present our results in Fig. 4 for a sequence of time moments from 5 to 20, and on two different grids. The upper row of panels contains the result, obtained on a uniform grid with $\Delta x = \Delta y = 30/128$. One can see that the nonlinearity is not strong enough without motion, and the initial elevation is transformed into a propagating cylindrical wave, similar to the one generated on a water surface when an object is dropped onto it. The lower row of panels contains the same solution, but computed on a finer grid with $\Delta x = \Delta y = 30/256$. The differences between the profiles for

the same time moments are small and compatible with the second-order truncation error. We have thus answered one of the pertinent physical questions.
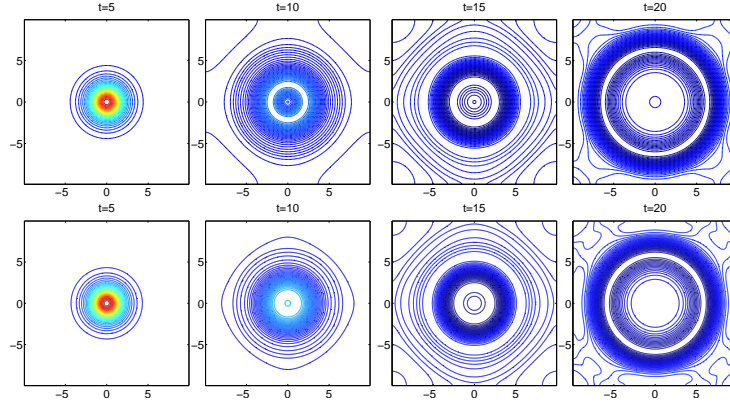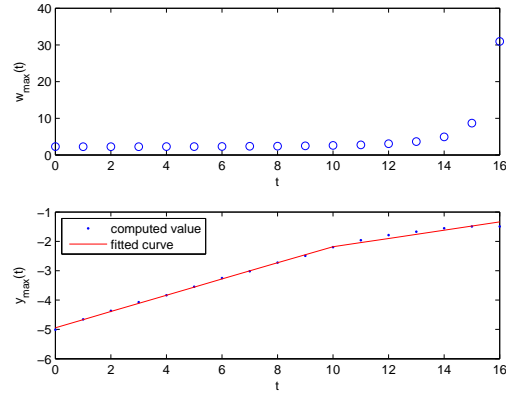


**Fig. 4** Evolution of the numerical solution of (1), (26) with $c = 0$ and $\eta = 0$, computed on two different grids

We now consider the case of a moderate phase speed $c = 0.3$ and compute the solution up to $t = 16$. The results are presented in Fig. 5. The top row of panels shows the lowest resolution ($\Delta x = \Delta y = 30/128$) solution, the plots in the middle row correspond to the medium resolution ($\Delta x = \Delta y = 30/256$), and the lowest row presents the results for the finest grid with $\Delta x = \Delta y = 30/512$. Clearly, the lowest resolution means that more numerical diffusion and dispersion are present, and as a result, the nonlinearity could not keep the shape in the form as prescribed by the initial condition. The interesting result obtained thanks to the numerical technology developed here, is that the soliton not only moves, but also evolves in a similar fashion as the standing soliton, resembling concentric cylindrical waves propagating outwards. In this case, however, the motion does not have a cylindrical symmetry because of the propagation of the solitary wave. The result is again a solitary structure, but of a different symmetry and with some kind of "aging", in the sense that the amplitude decreases in time, and the support increases.

In the middle row of panels in Fig. 5, we present the results obtained on a finer grid with $\Delta x = \Delta y = 30/256$. In this case, the numerical diffusion and dispersion are about four times smaller, and the nonlinearity was able to maintain the shape, prescribed in the initial conditions. This means that the shapes obtained in [5] may qualify as solitons. Unfortunately, the nonlinearity of BPE can lead to blowup even in the 1-D case (see the literature cited in [6]), if the initial condition has negative energy. There are no investigations concerning the possible blowup in 2-D, but in generic sense, one should expect a more stringent conditions on the initial energy in order to keep the shape from blowing up. The blowup can be clearly seen in the bottom row of Fig. 5, where the finest grid solution is shown, as well as in Fig. 6, where the maximum, $u_{max}$, of the soliton and its position, $y_{max}$, are traced in time.
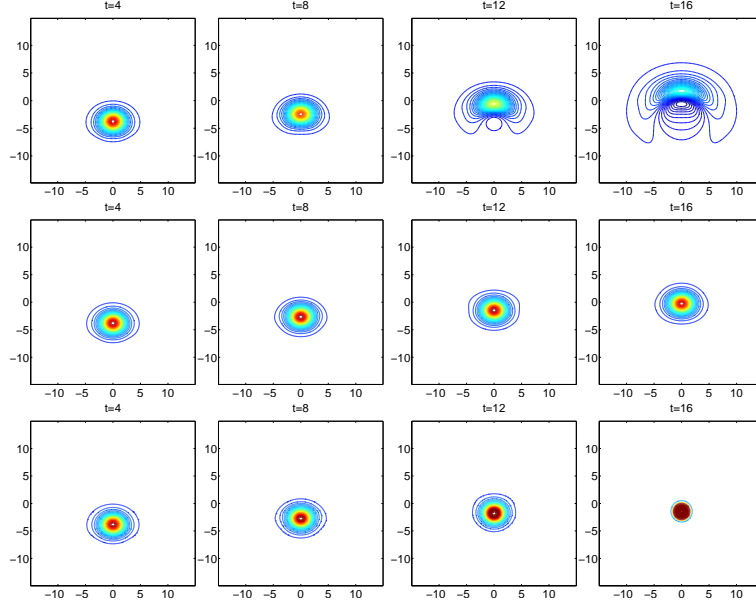
**Fig. 5** Evolution of the numerical solution of (1), (26) with $c = 0.3$ and $\eta = -5$



**Fig. 6** Evolution of the maximum of the solitary wave and its trajectory for the numerical solution shown in the bottom row of Fig. 5

One can see that at small times the maximum (as presented in the upper panel of Fig. 6) almost does not change and the slope of the trajectory (the lower panel of Fig. 6) is 0.28, which is within 5% from the expected theoretical value of 0.3. The disturbing news here is that at large times the maximum increases dramatically and a blowup takes place before $t = 17$.

This allows us to conclude that with the second-order nonlinearity of the BPE, one treads very thin path between the dispersion controlled evolution and blowup, and the selected mode of evolution depends on the grid resolution.

At the end, we consider the case of a larger phase speed $c = 0.7$, for which the computed solution is presented in Fig. 7. The nonlinearity is strong enough to keep the solution from dissipating, but the low scheme diffusion/dispersion cannot prevent the blowup, and the latter actually takes place much faster than in the case of the moderate phase speed $c = 0.3$.
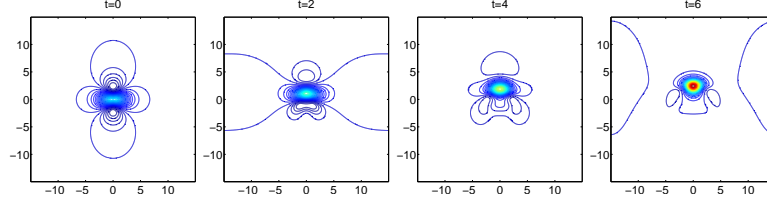


**Fig. 7** Evolution of the numerical solution of (1), (26) with $c = 0.7$ and $\eta = 0$, computed on a uniform grid with $\Delta x = \Delta y = 30/512$

## 5 Conclusion

In this paper, a novel idea is used to create an efficient finite volume scheme for the fourth-order generalized wave equations, such as the Boussinesq Paradigm Equation (BPE). A special change of dependent variables allows one to render the original problem to a system of the type encountered in compressible fluid dynamics. The scheme is validated by performing a series of mesh refinement studies. In treating several cases of single and interacting solitons in 1-D, the scheme has been demonstrated to be stable and robust.

In 2-D, different cases of physical significance are treated. *First*, the standing soliton has been investigated and we have demonstrated that it cannot survive and eventually will be transformed into a diverging propagating wave with cylindrical symmetry. *Second*, a solitary wave with moderate propagation speed is imposed as an initial condition and its evolution is numerically investigated. On the coarsest grid (largest numerical diffusion and dispersion), the propagating wave was transformed into a diverging wave skewed by the propagation. The medium grid allowed to trace the steady translation of the wave for long time period, but eventually the solutions blows up, signifying that the quadratic nonlinearity of BPE is not adequate for modeling permanent soliton-like waves. This conclusion is further confirmed by the computations on the finest grid, on which the blowup takes place earlier in time. *Third*, a case of large phase speed is investigated, and the same behavior is observed

as for the moderate phase speed with the only difference that the time scale of the blowup is much shorter.

# References

1. Boussinesq, J.V.: Théorie des ondes et des remous qui se propagent le long d'un canal rectangulaire horizontal, en communiquant au liquide contenu dans ce canal des vitesses sensiblement pareilles de la surface au fond. Journal de Mathématiques Pures et Appliquées **17**, 55–108 (1872)
2. Christou, M.A., Christov, C.I.: Localized waves for the regularized long wave equation via a Galerkin spectral method. Math. Comput. Simul. **69**, 257–268 (2005)
3. Christov, C.I.: Conservative difference scheme for Boussinesq model of surface waves. In: W.K. Morton, M.J. Baines (eds.) Proc. ICFD V, pp. 343–349. Oxford University Press (1995)
4. Christov, C.I.: An energy-consistent Galilean-invariant dispersive shallow-water model. Wave Motion **34**, 161–174 (2001)
5. Christov, C.I., Choudhury, J.: Perturbation solution for the 2D shallow-water waves. Mech. Res. Commun. (2009). Submitted
6. Christov, C.I., Velarde, M.G.: Inelastic interaction of Boussinesq solitons. J. Bifurcation & Chaos **4**, 1095–1112 (1994)
7. Gottlieb, S., Shu, C.W., Tadmor, E.: Strong stability-preserving high-order time discretization methods. SIAM Rev. **43**, 89–112 (2001)
8. Kurganov, A., Lin, C.T.: On the reduction of numerical dissipation in central-upwind schemes. Commun. Comput. Phys. **2**, 141–163 (2007)
9. Kurganov, A., Noelle, S., Petrova, G.: Semi-discrete central-upwind scheme for hyperbolic conservation laws and hamilton-jacobi equations. SIAM J. Sci. Comput. **23**, 707–740 (2001)
10. Kurganov, A., Polizzi, A.: Non-oscillatory central schemes for a traffic flow model with Arrhenius look-ahead dynamics. Networks and heterogeneous media To appear
11. Kurganov, A., Tadmor, E.: New high resolution central schemes for nonlinear conservation laws and convection-diffusion equations. J. Comput. Phys. **160**, 241–282 (2000)
12. Kurganov, A., Tadmor, E.: New high-resolution semi-discrete central scheme for hamilton-jacobi equations. J. Comput. Phys. **160**, 720–742 (2000)
13. Kurganov, A., Tadmor, E.: Solution of two-dimensional riemann problems for gas dynamics without riemann problem solvers. Numer. Methods Partial Differential Equations **18**, 584–608 (2002)
14. Lie, K.A., Noelle, S.: On the artificial compression method for second-order nonoscillatory central difference schemes for systems of conservation laws. SIAM J. Sci. Comput. **24**(4), 1157–1174 (2003)
15. Nessyahu, H., Tadmor, E.: Nonoscillatory central differencing for hyperbolic conservation laws. J. Comput. Phys. **87**(2), 408–463 (1990)
16. Zabusky, N.J., Kruskal, M.D.: Interaction of 'solitons' in collisionless plasma and the recurrence of initial states. Phys. Rev. Lett. **15**, 240–243 (1965)